GLL
Geomatics, Landmanagement and Landscape No. 2 • 2024, 195–216

ISSN 2300-1496 http://dx.doi.org/10.15576/GLL/2024.2.14

Research paper

Received: 26.03.2024
Accepted: 20.05.2024
Published: 31.07.2024

Multidisciplinary evaluation of geological, geotechnical, geomechanical, and hydrogeological parameters for assessing slope stability in the Aures Mountain Quarry

Abdeldjalil Mouerri[1, ✉] 0009-0004-2008-603x
Riheb Hadji[2] 0000-0002-9632-0812
Farid Zahri[2] 0009-0007-5183-9534
Younes Hamed[3] 0000-0001-7451-4459
Brahmi Serhane[1] 0000-0001-6371-8018

[1] Mining Engineering Department, Mining Institute, Echahid Cheikh Larbi Tebessi University; Mines Laboratory, Echahid Cheikh Larbi Tebessi University, Algeria
[2] Department of Earth Sciences, Institute of Architecture and Earth Sciences, Farhat Abbas University; Laboratory of Applied Research in Engineering Geology, Geotechnics, Water Sciences, and Environment, Farhat Abbas University, Algeria
[3] Department of Earth Sciences, Faculty of Sciences of Gafsa, University of Gafsa; International Association of Water Resources in the Southern Mediterranean Basin, Algeria
✉ Corresponding author: abdeldjalil.mouerri@univ-tebessa.dz

Summary

The study delves into characterizing the mechanical parameters of the Tahar Louchene aggregate quarry unit in Ain Touta municipality, Batna province, Algeria. This investigation is crucial to address recurring instabilities commonly encountered in open-cast mines. Our approach adopts a comprehensive methodology integrating geotechnical, geomechanical, and numerical analyses, aiming to provide a thorough assessment of fractured rock mass behavior. Our methodology begins with detailed geological surveys aimed at optimal drilling site selection. Geomechanical analysis follows, focusing on fracturing and evaluating rock mass quality, complemented by geotechnical investigations featuring in-situ testing. To gather representative samples, we extracted eighteen cylindrical cores (102 mm × 204 mm) from various benches using a mechanical coring drill. These cores underwent rigorous physical characterization, geochemical analysis, and mechanical testing. Furthermore, 3D FEM numerical modeling was applied to comprehensively assess rock edge stability. The outcomes of our study unveil the presence of four distinct discon-

tinuity sets within the primary formations, with particular emphasis on fault families of geological significance influencing deposit configuration. These fault structures provide valuable insights into stress history and tectonic evolution that directly impact the stability of the quarry. Moreover, our analysis identified various failure types, notably exacerbated by blasting practices that reduce safety factor values, highlighting the critical need for improved safety protocols. Our approach not only contributes to enhancing mining efficiency and productivity but also prioritizes the safety of equipment and personnel in open-cast mining operations across Algeria.

Keywords

open cast mine • stability • 3D FEM • GIS • RMR

1. Introduction

An open-cast mine represents a substantial ground excavation to extract valuable ore deposits, often extending extensively from the surface opening. The operational focus in mining endeavors prioritizes the seamless continuity of production, stringent workplace safety protocols, and astute economic considerations. This study embarks on a comprehensive exploration of slope stability along the rugged bench perimeters through a multidisciplinary approach encompassing field sampling, geomechanical parameter assessments, laboratory tests, and analytical calculations. By amalgamating these sophisticated methodologies, the primary objective is to evaluate slope stability while enhancing the foundational principles governing mine planning and berm/bench design.

The inherent mobility of rock masses underscores the dynamic nature of open-cast mining engineering, engendering uncertainties regarding the stability of resultant landforms. Consequently, the consideration of stability cannot be isolated from the overarching concerns of reliability and safety. Notably, prevailing geotechnical design practices in the mining domain often exhibit empirical underpinnings, diverging from the more analytical approaches observed in other geological engineering disciplines. Ground stability issues in open-cast mining are paramount, mirroring the criticality observed in other mining modalities albeit with distinct nuances. Adverse ground conditions can precipitate escalated operational costs, necessitating increased excavatability, heightened maintenance efforts, premature equipment replacement, or emergency remedial interventions. In contrast to underground mining, where alterations in ore removal sequences can trigger stability challenges due to the removal of ground support, open-cast mining confronts distinct safety and reliability implications when addressing stability concerns that impede original ore extraction.

Unfavorable ground conditions or stability challenges can imperil quarry safety and render certain land uses or geohazard mitigation strategies unfeasible. The multidisciplinary, interdisciplinary, and transdisciplinary assessments facilitate predictive insights, pre-emptive problem mitigation, optimization of ground conditions, and post-event ground condition rectification. Assessment methodologies serve as the fundamentals for design frameworks, often necessitating substantiation to mine management and engineers regarding the unsatisfactory ground conditions warranting remedial actions.

The presence of tectonic structures, such as faults, exerts profound implications on the geological configuration of mineral deposits, contributing to structural intricacies and influencing formation dynamics. Fault intersections engender a labyrinthine network of fractures and faults, influencing rock permeability, porosity, and fluid flow dynamics within the deposit. The orientation and characteristics of fault families furnish invaluable insights into stress histories, tectonic evolutions, and paleostress regimes, aiding in deciphering structural controls governing deposit formation and exploitation. Active fault zones or regions characterized by high strain rates elevate the risk of seismic events, slope instabilities, and geohazards, underscoring the imperative of comprehending fault families for safe and sustainable quarry resource exploitation.

Rock mass classification systems are indispensable tools in mining engineering problems, furnishing precise quantitative data and pragmatic guidelines for evaluating rock mass properties and structural parameters. Various geomechanical classifications, including Rock Mass Rating (RMR), Slope Mass Rating (SMR), Slope Rock Mass Rating (SRMR), Natural Slope Methodology (NSM), and Continuous Rock Mass Rating, are instrumental in assessing slope stability. The SMR system, an offshoot of the RMR system tailored for tunneling applications, incorporates correction factors to account for discontinuity orientations impacting slope stability.

In Jebel Ich Ali, the ENG Company exploits a limestone deposit with a mean hardness rating of 13 on the Protodiakonov scale. This study evaluates the stability of bench slopes within the Eastern zone of the quarry, proposing modifications to mining excavation designs to avert slope failures and their consequential impacts. This research aims to proffer enhanced solutions for fortifying slope stability and mitigating associated risks. The mining operations are meticulously structured to ensure the systematic extraction of valuable aggregates while meeting safety and environmental standards. This includes various methodologies and technological advancements for optimized efficiency and resource use. The core operation involves moving rocks methodically to spoil heaps, with machinery selection crucial for efficient and eco-friendly mining. Different methods are used based on deposit characteristics and efficiency, ranging from direct transport to spoil heaps to using trucks for processing. The blasting method is favored, mining from top to bottom on slopes and adapting to terrain complexities for safe and efficient resource extraction. The technological design considers rock properties, production targets, and environmental benchmarks, integrating processes like drilling, blasting, loading, transport, and concentration for efficient resource recovery. Critical elements include benches for operational access, dedicated working platforms, and evolving work fronts that adapt over time, showcasing the dynamic nature of mining in an open pit environment.

2. Study area

The limestone deposit under study is located within the Jebel Ich Ali region, Bled Tafrent, along the RN 03 road, approximately 10 km northeast of Ain Touta and 30 km from Batna. The site's geographical coordinates are 771 300 E longitudes, 3 925 400 N latitude, and an altitude of 1140 m above sea level (Fig. 1). The quarry's exploitation

involves a semi-trenched access opening with three operational levels, influenced by the monoclinal dip of the stratification. The quarry's location within the Aurès mountain range confers significant geological importance, warranting continuous evaluation of the geomechanical parameters to ensure efficient operations and optimal resource utilization [Benmarce et al. 2021]. This ongoing assessment is crucial for optimizing the extraction processes and maintaining the quarry's overall productivity.

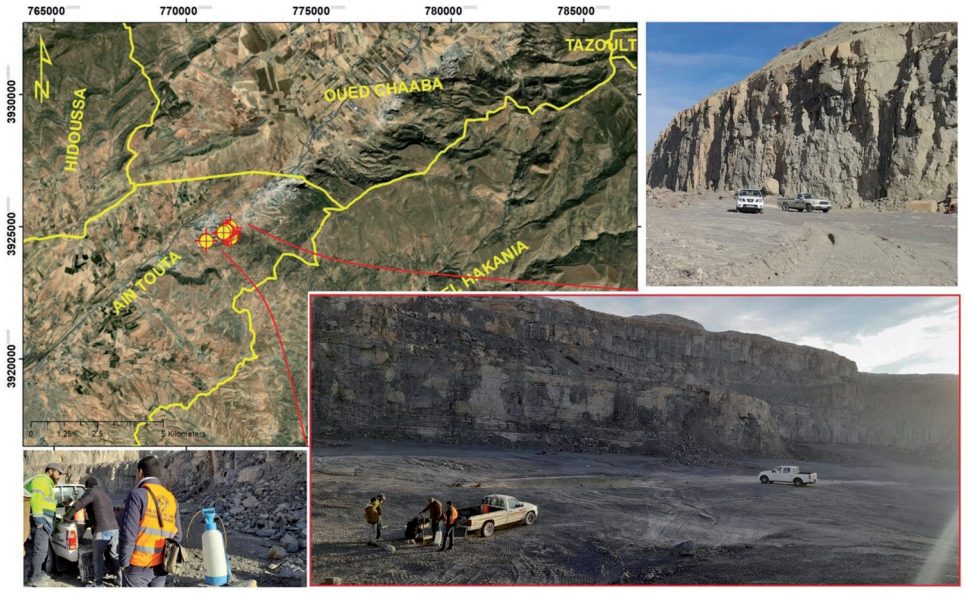

Source: Authors' own study

Fig. 1. Geographic location of the study area, with panoramic views of one of the quarries

2.1. Geological setting

The deposit's structure and tectonic characteristics include a general monoclinal dip towards the East at an angle of 7° and significant faults affecting the area to the west, north, and east, which delineate the deposit. The quarry area exhibits distinct geomorphological features, representing the southern flank of a perched synclinal flank with a sub-tabular monocline shape. This geological structure is characterized by layers of dark marly limestone interspersed with clay interbeds, dating back to the Turonian-Cenomanian period (Fig. 2).

The Turonian-Cenomanian geological formations are overlain by Senonian marls, Santonian limestones, and limestone slabs interlayered with gray Coniacian marls. The entire geological unit is further covered by Neogene deposits and Mio-Plio-Quaternary sediments. The region's structural influence is apparent through three main fault families affecting the massif. These faults significantly impact the geological configuration of the deposit, emphasizing the importance of evaluating mechanical parameters for

the efficient exploitation of the quarry. By delineating the lithological sequence in the deposit, geologists can gain insights into the composition, structure, and characteristics of the rock layers present. The observed lithological sequence in the deposit includes Upper Santonian Limestone, Coniacian Marly Limestone, Upper Turonian Limestone, and Dark Marly Limestone with Clay Interbeds from the Cenomanian. The lithological sections from the exposed outcrops in the field also include Mio-Plio-Quaternary and Neogene Formations, consisting of arable soil and tufa-limestone crust, on the Santonian Limestones (Fig. 3).

Source: Authors' own study

Fig. 2. a. Panoramic view of the outcropped formations on the three benches of the quarry. b. The synthetic stratigraphic log includes observed lithological units in the quarry benches

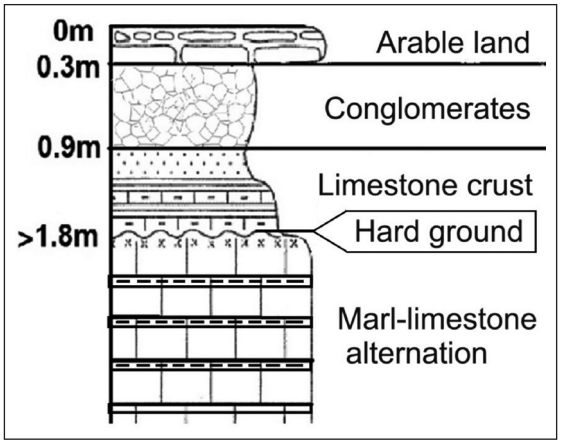

Source: Authors' own study

Fig. 3a. Lithological columns of the MPQ deposits

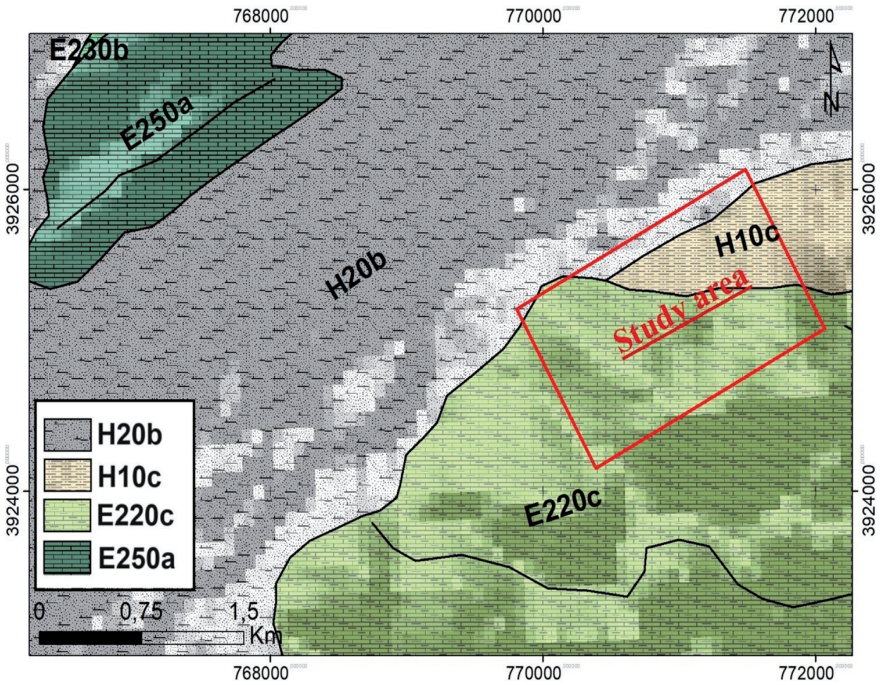

Legend:
H20b: Quaternary (Holocene): Current and recent alluvial deposits, occasional slope debris and piedmont accumulations (sand, gravel, and clay), and molasses.
H10c: Quaternary: Limestone crust – ancient Quaternary deposits with encrusted surface.
E220c: Upper Cretaceous (Turonian): Limestones and marls. Haut du formulaire.
E250a: Upper Cretaceous (Campanian and Maastrichtian): Marly assemblage at the base and diverse limestones (oolitic, fossiliferous, with flint) at the top.
E230b: Upper Cretaceous (Coniacian and Santonian): Limestones. Haut du formulaire

Source: Authors' own study

Fig. 3b. Simplified geological map of the study area

3. Material and methods

The methodology employed in our research combines three distinct approaches to quantitatively and qualitatively assess the stability of the quarry.

The first step involves fieldwork, which entails data acquisition along the quarry's face. The sampling method used for rock faces is the conventional traverse survey [Hadjigeorgiou et al. 1995], which allows for the collection of lithostratigraphic and morphostructural data for each geological layer (Fig. 2). Discontinuity characteristics are recorded and stored in a database. A compilation of azimuths and dip angles of recorded discontinuities along the entire quarry face is established. Geological parameters such as roughness and alteration are estimated by comparing the appearance of the discontinuity surface with standard profiles [Barton et al. 1974]. As for the physico-mechanical parameters, laboratory tests were conducted on rock samples from different geological formations.

A geometric approach, taking into account the information obtained from structural surveys, is used to characterize the main sets of discontinuities [Martin 2000]. This approach allows for the visualization of preferential families of discontinuities, revealing different potential instability modes through kinematic analysis. The software 'DIPS V.5.1' is utilized for this purpose. Internal friction angles of the various formations are derived from compression tests and validated using the 'RocLab-RocSciences' software.

The data resulting from the geometric analysis of different sets of discontinuities are then employed in the empirical approach to assess the quarry's stability. In this approach, the RMR (Rock Mass Rating) and SMR (Slope Mass Rating) classification systems are utilized. The RMR classification [Bieniawski 1993] allows for the evaluation of various parameters, each of which is assigned a coefficient. The sum of these coefficients determines the RMR value. This system encompasses five basic parameters: 1) uniaxial compressive strength of the rock, 2) RQD value for the rock mass, 3) spacing of discontinuities, 4) condition of discontinuities, and 5) hydraulic conditions.

The SMR classification [Romana 1993] is derived from the RMR classification by introducing a factor adjustment based on the relative orientation of discontinuities and the slope, as well as a correction factor based on the excavation method.

$$SMR = RMR_{basic} + (F1 \cdot F2 \cdot F3) + F4 \tag{1}$$

The coefficients F1, F2, F3, and F4 are determined from the Romana catalog [Romana et al. 2015]. SMR provides a description of rocks in five classes indicating their stability, potential failure modes, and recommended support.

The numerical approach relies on the finite element method using the Plaxis (3D) code, which enables the quantification of deformation and failure mechanisms. The mechanical parameters required for modeling are based on the RMR system and its empirical relationships. Thus, the properties of the rock mass are determined with equivalent characteristics.

The following expressions determine the equivalent Young's modulus (E), cohesion (c), and internal friction angle (φ) [Serafim and Pereira 1983, Bieniawski 1979, Trunk and Hönisch 1989].

$$E_{eq}\,(GPa) = 10(RMR - 10) / 40 \tag{2}$$

$$C_{eq}\,(kPa) = 5\,RMR \tag{3}$$

$$\varphi_{eq}\,(deg) = 0.5\,RMR + 8.3 \pm 7.2 \tag{4}$$

We performed a statistical analysis focusing on specific discontinuity parameters. This analysis allowed us to differentiate and measure the characteristics of each of the previously defined families. We utilized the XL-stat-Pro software for this purpose, enhancing the precision and depth of our findings.

By comparing the quantitative results obtained from these four approaches, the stability of the quarry slope can be qualitatively evaluated.

Source: Authors' own study

Fig. 4. Geological survey and fracture measurements of different outcrops

3.1. Sampling campaign

A sampling campaign was planned and executed to gather representative data from the quarry. A total of 18 intact core samples were extracted from diverse bench locations across distinct sectors of the quarry (Fig. 5), adhering to the guidelines outlined in ASTM D4220/D4220M, 'Standard Practices for Preserving and Transporting Soil Samples'. The sampling process employed a diamond-tipped mechanical coring machine (U-Test) with diameters of 82 and 102 mm, following ASTM D2113, 'Standard Practice for Rock Core Drilling and Sampling of Rock for Site Exploration'. These intact core samples were carefully preserved and transported to the laboratory for further analysis, as per ASTM D4220/D4220M. In the laboratory, the core samples underwent a series of mechanical tests, including uniaxial compressive strength, and tensile strength, assessments, following the procedures outlined in ASTM D7012, 'Standard Test Methods for Compressive Strength and Elastic Moduli of Intact Rock Core Specimens under Varying States of Stress and Temperatures'. The test results were meticulously analyzed and interpreted by a panel of experts to produce a comprehensive report on the geomechanical properties of the quarry rock mass [Raïs et al. 2017]. The sampling campaign and subsequent laboratory testing adhered to the standards of quality assurance and quality control, ensuring the reliability and reproducibility of the obtained data. The use of ASTM standards throughout the process guaranteed the adoption of recognized and accepted methodologies; facilitating the comparison of results with other studies and the integration of findings into the broader body of knowledge in the field of rock mechanics and slope stability analysis.

3.2. Geotechnical survey

The geotechnical survey employs standardized tests to evaluate soil and rock properties, facilitating geotechnical applications and query characterization.

The laboratory conducted Identification tests on non-rocky samples (N° 2, 4, 5, 6) to assess their properties. The particle size distribution test categorizes soil particles into size fractions, for understanding mechanical behavior and classifying soil based on sand, silt, and clay content. The Atterberg limits test determines soil consistency states such as liquid and plastic limits, for evaluating soil behavior under varying moisture conditions and informing foundation design. Additionally, the sand equivalent test assesses fines cleanliness in granular materials, ensuring construction quality control by evaluating the opacity of fine particles.

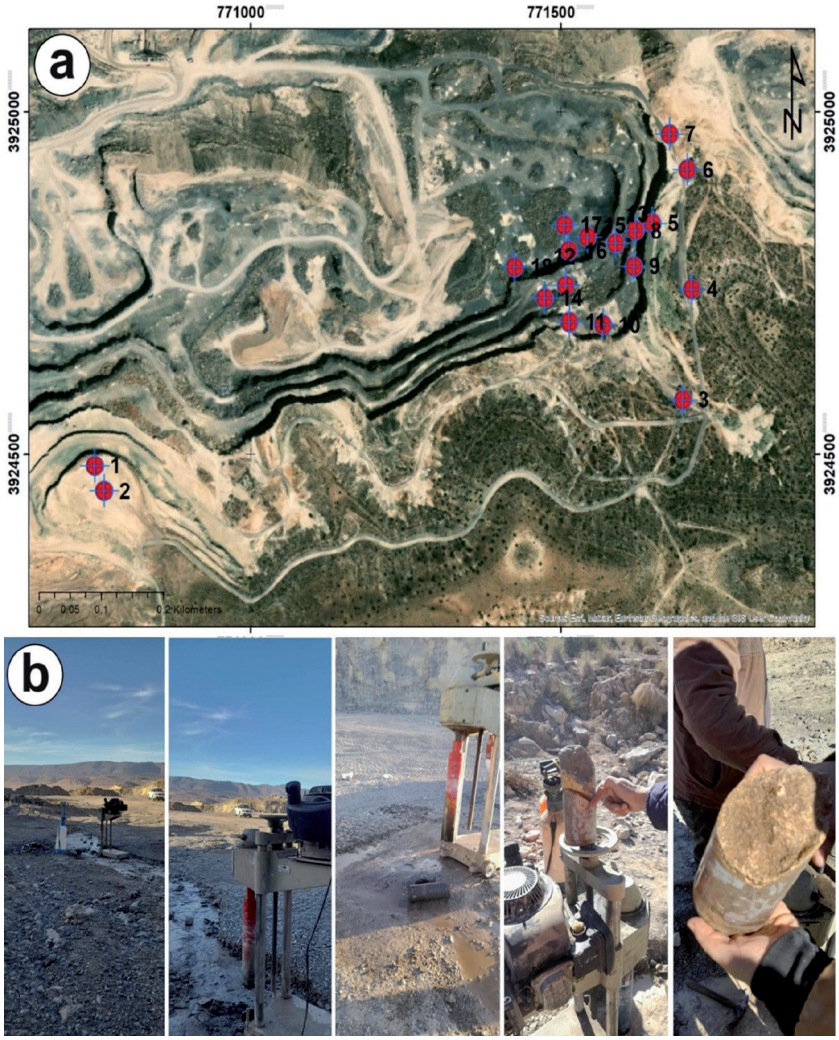

Source: Authors' own study

Fig. 5. a. Distribution of drilling/sampling locations in the quarry. b. Core drilling in different sectors

Uniaxial compression strength determination for rocky samples focused on limestone and marl rock samples. The procedure adhered to standard specifications, utilizing a uniaxial compression press equipment, displacement measurement device, loading device, and safety gear (Fig. 6). Samples were prepared representatively as per standard requirements, and the test procedure involved applying a progressive load until specimen fracture, recording load, and displacement data continuously, as per standard requirements. Results were analyzed to assess sample consistency and identify any significant variability in the quarry.

3.3. Geo-chemical analysis

The geochemical analysis protocol began with sample preparation, where collected rocks were ground into a fine powder using a suitable grinder to ensure homogeneity. This powdered material was then used to create pellets by pressing them at high pressure, resulting in compact and uniform samples for analysis. Calibration of the Energy Dispersive X-ray Fluorescence (EDXRF) device followed, involving the use of reference standards with known chemical elements to correct any instrumental variations and ensure the accuracy of results [Quye-Sawyer et al. 2015].

Subsequently, the mounted samples were placed into the calibrated EDXRF device for analysis. An X-ray beam was directed toward the samples, exciting atoms within them and causing the emission of characteristic fluorescent radiation. This emitted radiation was then measured to determine the chemical elements present in the samples.

The data obtained from this analysis were processed and analyzed to ascertain the concentrations of chemical elements in the samples.

Source: Authors' own study

Fig. 6. Mechanical test for uniaxial compression strength performed with a uniaxial compression press

3.4. 3D finite elements stability analysis

Geological engineering experts and institutions within the mining and geotechnical engineering sector rely on the advanced capabilities and functionalities offered by PLAXIS 3D, a powerful finite element method (FEM) software package. This state-of-the-art tool is instrumental in providing robust geotechnical solutions, particularly in critical slope stability assessment studies. Its sophisticated features and versatile modeling capabilities enable precise analysis and simulation of complex geological and geotechnical scenarios, ensuring accurate evaluations of slope stability and deformation behavior. In the studied case, the primary factor contributing to the potential for sliding is the presence of an intercalated marly layer intercalated between limestone formations. This geological configuration introduces a weak interface within the rock mass, potentially compromising overall slope stability. The slope geometry modeled in PLAXIS 3D features a step height of 15 me and a steep slope angle of 80°. The critical clay layer is specified with a thickness of 0.3 m and an inclination angle of 5°, reflecting the site-specific geological conditions. The mesh density is categorized as average, striking a balance between computational efficiency and spatial resolution to capture the essential features of the slope. The material properties assigned to the limestone and clay layers are based on laboratory test results and field observations, as documented in an internal company report. The limestone exhibits a volumetric specific weight (γ) of 2660 N/m^3, a wet weight (γ) of 20.58 N/m^3, cohesion (C) of 874 KPa, a friction angle (φ) of 26.15°, a Poisson's coefficient (υ) of 0.31, and a Young's modulus (E) of 73.10 GPa. In contrast, the clay material is characterized by a higher volumetric weight of 2690 N/m^3, a lower cohesion of 61 KPa, a friction angle of 10°, a Poisson's coefficient of 0.3, and a Young's modulus of 278 MPa. These geotechnical parameters are crucial inputs for the FEM stability analyses, enabling the simulation and prediction of slope behavior under various loading conditions and environmental factors. The Mohr-Coulomb constitutive model, widely used in geotechnical engineering, is particularly well-suited for this application, as it captures the interplay between material properties and slope stability.

By leveraging the advanced capabilities of PLAXIS 3D, geotechnical engineers can gain valuable insights into the potential failure mechanisms, safety factors, and deformation patterns of the studied slope. This is essential for designing effective stabilization measures, optimizing excavation sequences, and ensuring the overall safety and stability of the quarry operations.

4. Result and discussion

4.1. Physical characteristics

The measurements taken from a series of core samples provided average densities relative to dry weight and associated moisture contents, as shown in Table 1.

These data offer insights into the physical properties of the geological formations sampled, facilitating a comprehensive assessment of the structure and composition of materials within the quarry. The range of densities and moisture contents highlights the

variability in physical characteristics among different layers, crucial for directing the extraction and processing of aggregates.

Table 1. Physical characteristics of deposit formations

Sample type			Density [D]	Content [w] water
MPQ			**2.14**	**7.4**
Marl-Limestone alternation			**2.62**	**1.8**
Limestone			**2.66**	**2.1**
Marly limestone			**2.69**	**10.5**
Sieve [mm]	**%D Passing**			
	ECH 2	**ECH 4**	**ECH 5**	**ECH 6**
D_{max}	100	100	100	100
40	100	100	100	100
31.5	99	95	93	96
25	92	89	90	91
20	85	87	85	88
16	80	84	82	84
14	75	80	75	81
10	70	74	71	79
8	61	67	70	75
6,3	60	66	68	71
4	54	62	65	68
2	49	58	60	63
1	47	55	56	57
0.500	45	51	52	50
0.200	42	48	50	47
0.080	38	45	42	39
Sample	**LL**	**PL**	**PI**	**SE**
01	53.0	28.50	24.50	41
02	61	31	30	36
03	59	30.5	28.5	34
04	55	28	27	35

The analysis of density and water content shows that MPQ materials have a density of 2.14 and a water content of 7.4%, indicating recent formation with moderate porosity. The alternation between Marne and Limestone has a higher density of 2.62 and a lower water content of 1.8%, suggesting a more compact structure. Limestone itself has a density of 2.66 and a low water content of 2.1%, indicating a dense formation. Marly limestone has a density of 2.64 but a high-water content of 10.5%, suggesting less density but significant water retention capacity. The Atterberg limits and sand equivalent values for samples SMP 2, 4, 5, and 6 show variations in soil composition, with clayey soil indicated by higher plasticity index values. The relatively high sand equivalent values suggest a substantial proportion of fine particles, influencing soil compactness and permeability.

4.2. Geochemical and mineralogical characteristics

The geochemical analysis using X-ray fluorescence of samples from different sectors of the quarry reveals the following average chemical contents for each facies (Table 2):

Silica (SiO_2) varies between 1.99% and 11.51%. The highest silica content is found in marl and limestone alternation samples, while the lowest is in marly limestone samples.

Alumina (Al_2O_3) ranges from 0.7% to 5.50%. The highest alumina content is found in samples from marly limestone, while the lowest is in samples from limestone (top).

Iron Oxide (FeO) contents are generally low, ranging from 0.24% to 0.95%. The highest iron content is found in samples from the marl and limestone alternation.

Calcium Oxide (CaO) varies between 48.02% and 58.20%. The highest calcium content is found in samples from limestone (top), while the lowest is in samples from the marl and limestone alternation.

Sulfur Trioxide (SO_3) and Sodium + Potassium (Na_2OK_2O) contents are generally low, ranging from 0.12% to 0.45% and 0.18% to 0.85%, respectively.

Chlorine (Cl) contents are very low, on the order of a few milligrams per kilogram.

Magnesium Oxide (MgO) ranges from 0.55% to 0.91%. The highest magnesium content is found in samples from the marl and limestone alternation.

Lead-Zinc (Pb-Zn) levels are very low (0.001% to 0.002%), indicating a negligible presence of lead and zinc in the analyzed samples.

Loss on ignition, representing the weight loss of samples when heated to high temperature, ranges from 7% to 13%. This loss on ignition may be due to the presence of water or other organic or volatile compounds in the samples.

These results provide valuable insights into the chemical composition of samples in each studied facies. The variations in chemical contents, such as silica, alumina, and calcium oxide, highlight the diversity of geological formations within the quarry.

After conducting X-ray diffraction (XRD) analysis on the limestone formation represented by sample (N001) (Fig. 7), the primary mineral constituents were identified. The limestone is predominantly composed of calcite ($CaCO_3$), which accounts for approximately 84.6% of the sample when converted from the measured 49.1% CaO content. This high calcite content is typical of the purity limestone suitable for use as

an aggregate in concrete production. In addition to the dominant calcite phase, the limestone also contains quartz (SiO_2), and hematite (Fe_2O_3) as minor mineral components. Quartz, a common silicate mineral, contributes to the overall hardness and abrasiveness of the limestone aggregate. The presence of hematite, an iron oxide mineral, suggests some degree of oxidation or alteration within the deposit.

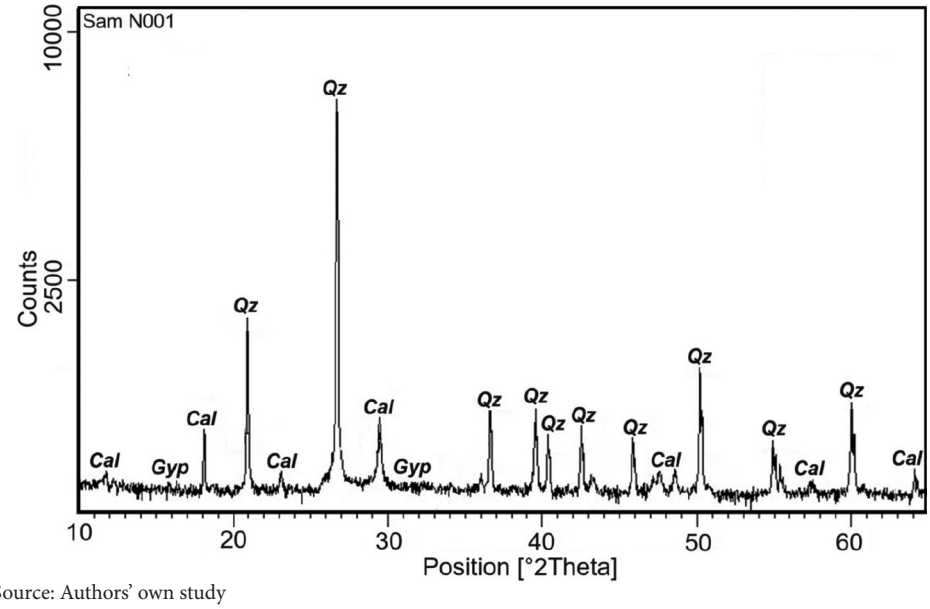

Source: Authors' own study

Fig. 7. X-ray diffraction (XRD) pattern of the limestone sample

Table 2. Results of geochemical composition analyses.

	SiO_2	Al_2O_3	FeO	CaO	SO_3	Na_2OK_2O	CL	MgO
Alternating marl and limestone	11.51	4.19	0.95	48.02	0.18	0.85	0.008	0.91
Limestone (summit)	2.33	0.7	0.38	58.20	0.15	0.20	0.006	0.86
Limestone (base)	5.04	1.3	0.70	53.87	0.45	0.50	0.010	0.80
Marly limestone	1.99	5.50	0.24	49.16	0.12	0.18	0.005	0.55

Note: The Pb-Zn rates are very low (0.001–0.002%). The loss on ignition is between 7–13%.
Note: The values presented in the results are average values

Gypsum ($CaSO_4 \cdot 2H_2O$), a hydrous calcium sulfate mineral, was also detected in trace amounts. The occurrence of gypsum may be attributed to the interaction between sulfur-bearing fluids and the carbonate rock or the presence of evaporitic deposits within the limestone formation.

The identification of these mineral phases through XRD analysis provides valuable insights into the petrographic composition of the limestone aggregate. This information is crucial for understanding the physical, chemical, and mechanical properties of the rock.

4.3. Mechanical characteristics

The mechanical properties of various rock samples, including their facies, compression strength (CS), and tensile strength (TS), were analyzed through simple compression tests, with the results presented in Table 3.

Table 3. Results of compression tests on different samples

Sample	Facies	Stratigraphy	CS [MPa]	TS [MPa]
1	Marly limestone in flakes	Oligocene roof	21.2	2.3
2	Recent alluvial deposits (Friable)	MPQ	NM	NM
3	Marly limestone in flakes	Oligocene roof	23.4	2.4
4	Recent alluvial deposits (Friable)	Neogene	NM	NM
5	Deposit (Friable)	MPQ	NM	NM
6	Recent alluvial deposits (Friable)	Neogene roof	NM	NM
7	Limestone	Santonian	59.3	6.5
8	Limestone	Santonian	58.9	4.6
9	Limestone slabs intercalated with gray marl	Coniacian	50.2	5.3
10	Limestone slabs intercalated with gray marl	Coniacian	49.2	5.1
11	Limestone slabs intercalated with gray marl	Coniacian	48.0	4.7
12	Medium-grained bioclastic limestone	Turonian	63.8	2.2
13	Medium-grained bioclastic limestone	Turonian	62.1	2.1
14	Medium-grained bioclastic limestone	Turonian	65.4	6.2
15	Dark marly limestone with clay interbeds	Cenomanian	23.6	2.3
16	Dark marly limestone with clay interbeds	Cenomanian	24.9	2.3
17	Dark marly limestone with clay interbeds	Cenomanian	23.5	2.1
18	Dark marly limestone with clay interbeds	Cenomanian	25.1	2.3

Interpretation of results:

Samples 1, 3, and 7 to 18 primarily consist of limestone with diverse characteristics, ranging from friable marly limestone to medium-grained bioclastic limestones and dark marly limestone with clay interbeds.

Samples 2, 4, 5, and 6 are recent alluvial deposits, exhibiting a friable structure with non-measurable (NM) resistance values.

Compression (CS) and tensile (TS) strengths are expressed in Megapascals (MPa) and vary significantly among different samples.

Samples 7, 8, 9, 10, 12, 13, and 14 demonstrate relatively high compression strengths, indicating their ability to withstand significant loads, ensuring stability, and possessing acceptable quality and characteristics for produced aggregates.

Compression strength often exceeds tensile strength (TS = CS · 1/10), a typical trait for most rock types.

Medium-grained bioclastic limestone samples (12, 13, 14) exhibit high compression strengths, suggesting a solid and compact structure.

Dark marly limestone with clay interbed samples (15, 16, 17, 18) show relatively lower compression and tensile strengths.

These results provide crucial insights into the mechanical properties of rock samples, which are essential for design considerations in geotechnical contexts. Understanding the mechanical properties of rocks, such as their compression and tensile strengths, is crucial for assessing their stability, suitability for various applications, and potential risks in geotechnical and geomaterial contexts.

4.4. Geometrical and geomechanical approach

The stereographic projection considers all discontinuity families, slope orientation, and friction angle. Results from this analysis delineate different families for each facies alongside the associated modes of failure. The Santonian and Turonian limestones exhibit significant faults with NE and NW dips. Field measurements reveal four major faults with directions ranging from 110° to 200°. Stereographic projection of these fault planes (Fig. 8) allows deducing various failure possibilities: wedge failure at the intersection of faults [F1 · F2 with a dip of 75°], [F1 · F3, 60°], [F2 · F3, 60°], and [F3 · F4, 62°]. Fault 3 (60/200) presents the possibility of planar sliding.

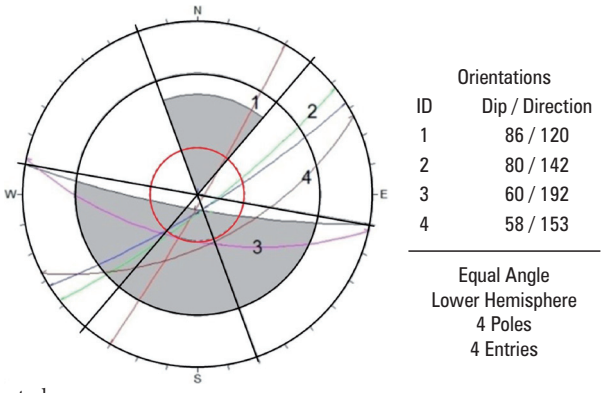

Source: Authors' own study

Fig. 8. Kinematic analysis through the stereographic projection of the limestone career

The statistical analysis of 422 discontinuity measurements taken on the quarry face unveils four main discontinuity families across the three facies of the study site. Results stem from compiling 30 structural surveys per traverse, processed using 'DIPS 5.1' software. Kinematic analysis delineates different modes of rock slope failures, including planar sliding, wedge failure, and toppling.

4.5. Empirical approach

This study employs the SMR to assess the quarry's stability. The analysis reveals a significant risk of instability within the quarry, especially in areas with marly intercalations where wedge and planar failure modes are prevalent. These findings emphasize the critical need for targeted stability measures and continuous monitoring protocols in such geotechnical environments to mitigate potential hazards and maintain safe operational conditions.

The Santonian Limestone, characterized by an RQD of 13 and a discontinuity spacing of 20, demonstrates moderate RMR and SMR values of 62 and 42.7, respectively, indicating a reasonable stability level. However, its partial stability rating raises concerns about potential instability, attributed to the presence of vertical joints and numerous wedges within the rock mass, suggesting a potential failure mode associated with these features.

Similarly, the Coniacian Interbedded Marl-Limestone shares similarities with the Santonian Limestone regarding RQD (12) and discontinuity spacing (20), as well as moderate RMR (68) and SMR (48.7) values. Like the Santonian Limestone, it also receives a partial stability rating, although specific geological features contributing to this rating are not explicitly detailed.

Lastly, the Cenomanian Bioclastic Limestone exhibits the highest RQD of 14 and favorable RMR (76) and SMR (56.7) values among the formations, indicating superior rock quality and stability potential. However, it is also rated as moderately and partially stable, highlighting potential instability factors not specified in the data provided. This underscores the necessity for comprehensive site assessments and continuous monitoring to address potential stability challenges effectively in quarry operations.

4.6. FEM modeling approach

Using Finite Element Method (FEM) analysis, we conducted simulations to assess the stability of the quarry face under different scenarios and calculated the resulting safety factors. The first scenario involved modeling the limestone step at the 1080 m level without considering the presence of a clay layer intercalation, while the second scenario included the clay layer at the 1065 m level. Our simulations, conducted using the computational code 'Plaxis 3D,' yielded insightful results. In the absence of the clay layer, the safety factor (FS) was notably high (FS > 1.5), indicating the stability of the limestone step at 1080 m without clay intercalation. However, when incorporating the clay layer, the modeling showed marginal stability with a safety factor below 0.54,

particularly under wet conditions, highlighting the potential for instability and suggesting the necessity of implementing a drainage system. The poor mechanical properties of the clay layer were identified as a significant factor contributing to potential mass movement.

To address this issue, we proposed adjustments to the geometric parameters of the bench, assuming dry conditions for the clay layer. Specifically, for the profile at the 1065 m level, we recommended reducing the step height to 9 m and lowering the slope angle to 70°. Upon implementing these adjustments, a substantial improvement in the safety factor was observed, reaching a value of 1.78, thereby enhancing slope stability and validating the effectiveness of this proposed solution. Notably, this improvement was achieved through the reduction of geometric parameters, underscoring the importance of geometric design in slope stability management (Fig. 9).

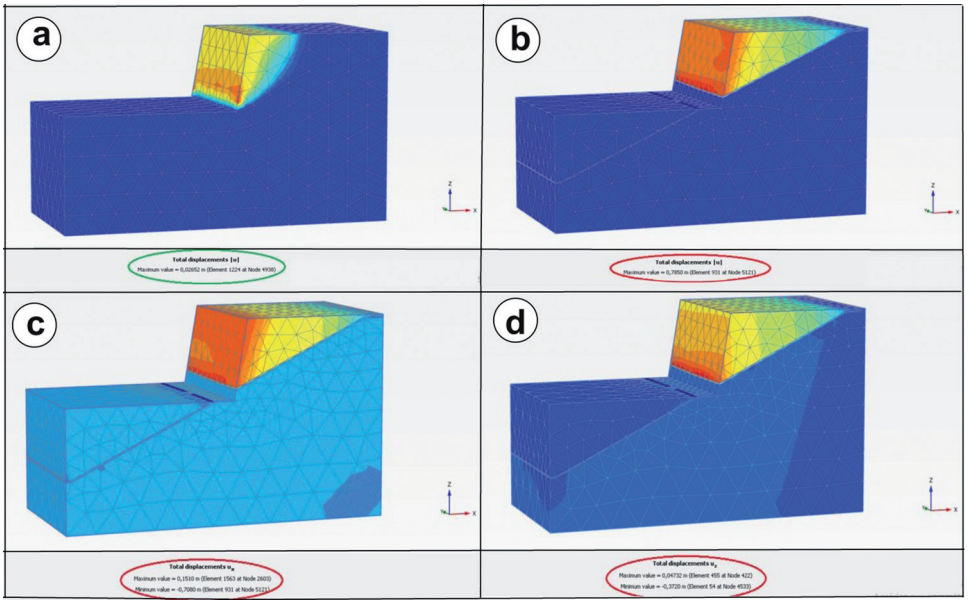

Source: Authors' own study

Fig. 9. a. Total displacement. b. Deviatoric displacement. c. Horizontal displacement. d. Vertical displacement

Comparing the simulation results without clay intercalation (safety factor of 8.67 and total displacement of 0.02 m) to those with clay intercalation (safety factor of 0.54 and total displacement of 0.78 m) emphasizes the significant impact of the proposed solution. With our recommended adjustments, the safety factor improved to 1.78, and the total displacement was reduced to 0.1 m (Fig. 10). This detailed analysis highlights the efficacy of the proposed solution in enhancing slope stability and reducing displacement, crucial considerations in geotechnical engineering assessments.

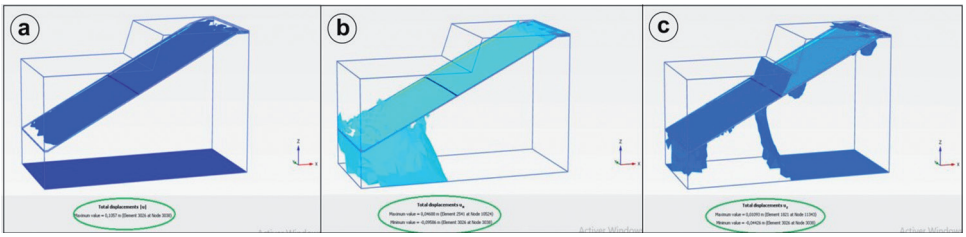

Source: Authors' own study

Fig. 10. a. Total displacement (Umax). b. Horizontal displacement (Ux). c. Vertical displacement (Uz)

5. Conclusions

The research work conducted at the Tahar Louchene aggregate Quarry has revealed interesting findings across geological, geotechnical, and geochemical dimensions at the site.

Geographical significance: Nestled within Jebel Ich Ali, the quarry holds notable geological significance. Its distinctive topography, featuring three exploitation levels, plays a pivotal role in influencing extraction methods and material processing strategies.

Mechanical parameters: Uniaxial compression tests on representative samples have revealed a range of mechanical characteristics. Medium-grained bioclastic limestone exhibits high compression strength, indicative of robust structural quality. Conversely, dark marly limestone with clay interbeds displays lower strengths, highlighting varied mechanical properties.

Geological features: The site's geological profile, spanning from Turonian-Cenomanian to Neogene and MPQ formations, showcases significant lithological diversity. Structural faults, including four main fault families, directly impact the quarry's geological structure, underlining the necessity of assessing mechanical parameters for efficient exploitation.

Geochemical characteristics: Through analysis of geological formations, essential insights into chemical properties crucial for quarry exploitation have been gleaned. Variations in constituent elements such as silica, alumina, calcium, sulfur, and magnesium oxide contribute to a comprehensive understanding of the formations' chemical composition.

The numerical modeling has yielded a realistic mechanical response, contingent upon factors such as model size, mesh dimensions, behavior model, boundary conditions, and material properties. Analysis without clay intercalation indicates high stability (FS = 8.67), whereas with clay intercalation, instability is observed (FS = 0.54). Adjusting geometric parameters leads to stability (FS = 1.78), with PLAXIS 3D modeling results endorsing reduced step height and slope angle to bolster stability.

This study lays a robust foundation for informed decision-making and future planning of extraction and material processing operations at the quarry.

References

Amamria S., Bensalem H., Taib H., Bensalem M.S., Hadji R., Hamed Y. 2023. Relationship between gravitational flap structures in the backlimb of anticlinal breakthrough Fault-Propagation Folds: case study of the Southern-Central Tunisian Atlas. Journal of Mountain Science, 20(12), 3525–3541. https://doi.org/0.1007/s11629-023-8265-5

Atif Y., Soulaimani A., Ait Lahna A., Yaagoub D., Youbi N., Pour A.B., Hashim M. 2022. Structural analysis and paleostress evolution in the Imiter silver mining region, Eastern Anti Atlas, Morocco: implications for mineral exploration. Minerals, 12(12), 1563. http://dx.doi.org/10.3390/min12121563

Barton N., Lien R., Lunde J. 1974. Engineering classification of rock masses for the design of tunnel support. Rock Mechanics, 6(4), 189–236.

Bedri K., Hamou M.O., Filali M., Hadji R., Taib H. 2023. Optimizing the blast fragmentation quality of discontinuous rock mass: Case study of Jebel Bouzegza Open-Cast Mine, North Algeria. Mining of Mineral Deposits, 17(4), 35–44. http://dx.doi.org/10.33271/mining17.04.035

Benmarce K., Hadji R., Zahri F., Khanchoul K., Chouabi A., Zighmi K., Hamed Y. 2021. Hydrochemical and geothermometry characterization for a geothermal system in semiarid dry climate: The case study of Hamma spring (Northeast Algeria). Journal of African Earth Sciences, 182, 104285.

Benyoucef A., Gadri L., Hadji R., Mebrouk F., Harkati E. 2022. Mining operations and geotechnical issues in deep hard rock mining – case of Boukhadra iron mine. Geomatics, Landmanagement and Landscape, 4, 27–46. http://dx.doi.org/10.15576/GLL/2022.4.27

Benyoucef A.A., Gadri L., Hadji R., Slimane H., Mebrouk F., Hamed Y. 2023. Empirical graphical and numerical model for the schematization of underground mining operations in the heterogeneous rock masses, case of Boukhadra mine, Algeria. Arab. J. Geosci., 16(3), 165. http://dx.doi.org/10.1007/s12517-023-07620-2

Bieniawski Z.T. 1979. Engineering classification of jointed rock masses. Trans. S. Afr. Inst. Civ. Eng., 15, 335–344.

Bieniawski Z.T. 1989. Engineering rock mass classifications: a complete manual for engineers and geologists in mining, civil, and petroleum engineering. John Wiley & Sons.

Bieniawski Z.T. 1993. Classification of rock masses for engineering: the RMR system and future trends. In: Rock Testing and Site Characterization, 553–573. Pergamon.

Boulemia S., Hadji R., Hamimed M. 2021. Depositional environment of phosphorites in a semiarid climate region, case of El Kouif area (Algerian-Tunisian border). Carbonates and Evaporites, 36(3), 53.

Bouragba N., Hadji R., Chouabbi A. 2023. An AHP GIS-based Methodology for the Stability Assessment of the Djebel El Ouahch Collapsees on the Numidian Flysh Formation in Northeast Algeria's Constantine Region. Central European Journal of Geography and Sustainable Development, 5(2), 24–45. http://dx.doi.org/10.47246/CEJGSD.2023.5.2.2

Dahoua L., Usychenko O., Savenko V.Y., Hadji R. 2018. Mathematical approach for estimating the stability of geotextile-reinforced embankments during an earthquake. Mining Science, 25, 207–217.

Fredj M., Hafsaoui A., Riheb H., Boukarm R., Saadoun A. 2020. Back-analysis study on slope instability in an open pit mine (Algeria). Scientific Bulletin of National Mining University, 2. http://dx.doi.org/10.33271/nvngu/2020-2/024

Gadri L., Hadji R., Zahri F., Benghazi Z., Boumezbeur A., Laid B.M., Raïs K. 2015. The quarries edges stability in opencast mines: a case study of the Jebel Onk phosphate mine, NE Algeria. Arabian Journal of Geosciences, 8, 8987–8997.

Guglielmi Y., Nussbaum C., Cappa F., De Barros L., Rutqvist J., Birkholzer J. 2021. Field-scale fault reactivation experiments by fluid injection highlight aseismic leakage in caprock analogs: Implications for CO_2 sequestration. International Journal of Greenhouse Gas Control, 111, 103471. http://dx.doi.org/10.1016/j.ijggc.2021.103471

Hadji R., Chouabi A., Gadri L., Raïs K., Hamed Y., Boumazbeur A. 2016. Application of linear indexing model and GIS techniques for the slope movement susceptibility modeling in Bousselam upstream basin, Northeast Algeria. Arabian Journal of Geosciences, 9, 1–18.

Hadji R., Rais K., Gadri L., Chouabi A., Hamed Y. 2017. Slope failure characteristics and slope movement susceptibility assessment using GIS in a medium scale: a case study from Ouled Driss and Machroha municipalities, Northeast Algeria. Arabian Journal for Science and Engineering, 42, 281–300.

Hadjigeorgiou J., Lessard J.F., Flament F. 1995. Characterizing in-situ block size distribution using a stereological model. Canadian tunnelling, 111–121.

Hamed Y., Khelifi F., Houda B., Sâad A.B., Ncibi K., Hadji R., ... Hamad A. 2023. Phosphate mining pollution in southern Tunisia: environmental, epidemiological, and socioeconomic investigation. Environment, Development and Sustainability, 25(11), 13619–13636. https://doi.org/10.1007/s10668-022-01888-1

Hemeda S. 2021. Geo-environmental monitoring and 3D finite elements stability analysis for site investigation of underground monuments. Horemheb tomb (KV57), Luxor, Egypt. Heritage Science, 9(1), 17.

Kallel A., Ksibi M., Dhia H.B., Khélifi N. (eds.). (2018). Recent advances in environmental science from the Euro-Mediterranean and surrounding regions: Proceedings of Euro-Mediterranean Conference for Environmental Integration (EMCEI-1), Tunisia 2017. Cham: Springer International Publishing. https://doi.org/10.1007/978-3-319-70548-4

Karim Z., Hadji R., Hamed Y. 2019. GIS-based approaches for landslide susceptibility prediction in Setif Region (NE Algeria). Geotechnical and Geological Engineering, 37(1), 359–374. https://doi.org/10.1007/s10706-018-0642-7

Kerbati N.R., Gadri L., Hadji R., Hamad A., Boukelloul M.L. 2020. Graphical and numerical methods for stability analysis in surrounding rock of underground excavations, example of Boukhadra Iron Mine NE Algeria. Geotechnical and Geological Engineering, 38, 2725–2733. https://doi.org/10.1007/s10706-020-01268-w

Mahleb A., Hadji R., Zahri F., Boudjellal R., Chibani A., Hamed Y. 2022. Water-borne erosion estimation using the Revised Universal Soil Loss Equation (RUSLE) model over a semiarid watershed: Case study of Meskiana Catchment, Algerian-Tunisian Border. Geotechnical and Geological Engineering, 40(8), 4217–4230. http://dx.doi.org/10.1007/s10706-022-01929-x

Maino M., Decarlis A., Felletti F., Seno S. 2013. Tectono-sedimentary evolution of the Tertiary Piedmont Basin (NW Italy) within the Oligo-Miocene central Mediterranean geodynamics. Tectonics, 32(3), 593–619. https://doi.org/10.1002/tect.20035

Martin G. 2000. Conception des excavations minières souterraines à l'aide de la modélisation de réseaux de discontinuités. Thèse présentée à l'Université Laval, Québec, Canada, 163 p.

Pantelidis L. 2009. Rock slope stability assessment through rock mass classification systems. International Journal of Rock Mechanics and Mining Sciences, 46(2), 315–325. https://doi.org/10.1016/j.ijrmms.2008.07.003

Quye-Sawyer J., Vandeginste V., Johnston K.J. 2015. Application of handheld energy-dispersive X-ray fluorescence spectrometry to carbonate studies: Opportunities and challenges. Journal of Analytical Atomic Spectrometry, 30(7), 1490–1499. https://doi.org/10.1039/c5ja00096f

Raïs K., Kara M., Gadri L., Hadji R., Khochman L. 2017. Original approach for the drilling process optimization in open cast mines: Case study of Kef Essenoun open pit mine Northeast of Algeria. Mining Science, 24, 147–159. https://doi.org/10.5262/ms/2017242

Romana M. 1991. SMR classification. In: ISRM Congress, September. ISRM.

Romana M. 1993. A geomechanical classification for slopes: Slope mass rating. Comprehensive Rock Engineering, 3(1), 575–599.

Romana M., Tomás R., Seron J.B. 2015. Slope mass rating (SMR) geomechanics classification: Thirty years review. In ISRM Congress, May, ISRM.

Saadoun A., Yilmaz I., Hafsaoui A., Hadji R., Fredj M., Boukarm R., Nakache R. 2020. Slope stability study in quarries by different approaches: Case Chouf Amar Quarry, Algeria. In: IOP Conference Series: Materials Science and Engineering, 960, 4, p. 042026). IOP Publishing. https://doi.org/10.1088/1757-899X/960/4/042026

Saadoun A., Fredj M., Boukarm R., Hadji R. 2022. Fragmentation analysis using digital image processing and empirical model (KuzRam): A comparative study. Journal of Mining Institute. https://doi.org/10.5262/jmi.2022190.

Şen Z., Sadagah B.H. 2003. Modified rock mass classification system by continuous rating. Engineering Geology, 67(3–4), 269–280.

Serafim J.L., Pereira J.P. 1983. Considerations of the geomechanics classification of Bieniawski. In: Proceedings international symposium engineering geology and underground construction, 1, 1133–1142.

Shuk T. 1994. Key elements and applications of the natural slope methodology (NSM) with some emphasis on slope stability aspects. In: Proceedings of the 4th South American Congress on Rock Mechanics, 2, 955–960.

Trunk U., Hönisch K. 1989. Cited at rock mechanics design in mining and tunneling, Bieniawski, p. 183.

Zahri F., Boukelloul M.L., Hadji R., Talhi K. 2016. Slope stability analysis in open pit mines of Jebel Gustar career, NE Algeria – A multi-steps approach. Mining Science, 23, 137–146. https://doi.org/10.5262/ms/2016223

Zeqiri R.R., Riheb H., Karim Z., Younes G., Rania B., Aniss M. 2019. Analysis of safety factor of security plates in the mine 'Trepça' Stantërg. Mining Science, 26, 21. https://doi.org/10.5262/ms/2019261

Zerzour O., Gadri L., Hadji R., Mebrouk F., Hamed Y. 2020. Semi-variograms and kriging techniques in iron ore reserve categorization. Application at Jebel Wenza deposit. Arabian Journal of Geosciences, 13, 1–10. https://doi.org/10.1007/s12517-020-05723-3

Zerzour O., Gadri L., Hadji R., Mebrouk F., Hamed Y. 2021. Geostatistics-based method for irregular mineral resource estimation. In: Ouenza Iron Mine, Northeastern Algeria. Geotechnical and Geological Engineering, 1–10. https://doi.org/10.1007/s10706-021-01859-5

Test Standards

Standard NF EN ISO 17892-4: Determines particle size distribution by sieving.
Standard NF EN ISO 17892-5: Tests water content, retractability, and swelling characteristics.
Standard NF EN ISO 17892-12: Determines Atterberg limits.
Standard NF P94-051: Laboratory testing methods for Atterberg limits.
Standard NF EN 933-8: Conducts the sand equivalent test.
Standard NF EN 933-6: Determines particle size distribution and fine elements content.
Uniaxial compression strength NF P94-420